Supplementary information

1. Characterization

The crystal structures of $Bi_4O_5Br_2$ and $Bi/Bi_4O_5Br_2$ were determined by X-ray diffractometry (XRD) on a SmartLabTM 9 kW instrument employing Cu-Kα irradiation (λ = 1.5416 Å) and operated in continuous mode, scanning the 2θ range from 10° to 70° with a step size of 0.02°/ min. The operating voltage and current were maintained at 30 kV and 20 mA, respectively.

Scanning electron microscopy (SEM) on an instrument was performed to observe the morphological features of $Bi_4O_5Br_2$ and $Bi/Bi_4O_5Br_2$. Each dry powder sample was placed in a tube with ethanol (1 mL) and dispersed for 30 min. The suspensions were then dropped onto a copper mesh and dried under an infrared lamp prior to inspection by SEM.

Transmission electron microscopy (TEM) was performed with a JEOL JEM-F200 instrument to study the dimensions of $Bi_4O_5Br_2$ and $Bi/Bi_4O_5Br_2$. Each dry powder sample was placed in a tube with ethanol (1 mL) and dispersed for 5 min. The suspensions were dropped onto a copper mesh and dried under an infrared lamp prior to inspection by TEM.

High-resolution transmission electron microscopy (HRTEM) was performed with a JEM-2100 F instrument (Hitachi, Japan) to determine lattice spacings. Complementary to SEM, energy-dispersive spectroscopy (EDS；ZEISS Sigma 300, Germany) and element distribution mapping were executed to provide a comprehensive elemental analysis.

UV/Vis/NIR absorption spectra of $Bi_4O_5Br_2$ and $Bi/Bi_4O_5Br_2$ were acquired on a Hitachi U-4100 spectrophotometer. All measurements were made at a scan speed of

200 nm min–1 in the range 200–1600 nm. Electron spin resonance (ESR) spectra of $Bi_4O_5Br_2$ and $Bi/Bi_4O_5Br_2$ were acquired on an A300 spectrometer (Bruker, Germany). Dimethyl pyridine N-oxide (DMPO) served as a trapping agent for superoxide and hydroxyl radicals, and 2,2,6,6-tetramethylpiperidine (TEMP) served as a trapping agent for singlet oxygen.

2. Cell Viability Assay

The biological safety of $Bi/Bi_4O_5Br_2$ nanosheets was evaluated by culturing cells in vitro. Briefly, BEAS-2B and NCM460 cells were cultured until they reached 80–90 % of their maximum cell density, and were then transferred to 96-well plates and cultivated at 37 °C in a CO_2 incubator for 24 h. They were then co-cultured with $Bi_4O_5Br_2$ and $Bi/Bi_4O_5Br_2$ at concentrations of 250, 500, 1000, 2000 and 4000 μg/mL for 24 h. Some cells were illuminated with light from a xenon lamp (500 W, 60 min), while others were kept in the dark. Cell viability was determined by a Cell Counting Kit-8 (CCK-8) assay.

3. Cells Live/dead Staining

To assess cell viability, BEAS-2B and NCM460 cells were stained using a calcein/propidium iodide (PI) cell viability/cytotoxicity assay kit. The stained cells were observed under an inverted fluorescence microscope (Axio Scope A1) for qualitative analysis.

4. Hemocompatibility assay

Fresh whole blood from healthy people was injected into tubes containing sodium citrate and diluted with 0.9% NaCl solution (4:5). Aliquots (10 mL) of distilled water (positive control), normal saline (negative control), $Bi_4O_5Br_2$ solution, and $Bi/Bi_4O_5Br_2$ solution were incubated in a series of tubes at 37 °C for 30 min. Thereafter, aliquots (0.2 mL) of the diluted blood solution were added to the respective media, and the

mixtures were cultured for 1 h. After centrifugation for 10 min at 2000 rpm, the supernatant was transferred to a 96-well plate. Following an enzyme-labeling procedure, optical densities (OD) were measured at 550 nm. The hemolysis rate ratio was calculated according to the following equation:

$$Antibacterial\ rate(\%) = \frac{[OD(sample) - OD(negative)]}{[OD(positive) - OD(negative)]} * 100\%$$

5. In Vitro Antibacterial Experiments

The antimicrobial efficacies of $Bi_4O_5Br_2$ and $Bi/Bi_4O_5Br_2$ was assessed using *E. coli* (ATCC 25922) and *S. aureus* (ATCC 2205SE0219). Firstly, the number of bacteria was adjusted to 1×10^6 CFU/mL, and the concentration of each sample was 2000 μg/mL. The bacterial suspensions were then mixed with aliquots (1 mL) of $Bi_4O_5Br_2$ and $Bi/Bi_4O_5Br_2$ solutions, respectively. As a control, normal saline (1 mL) was added to the bacterial suspension. All samples were then illuminated vertically with light from a 500 W xenon lamp ($\lambda > 420$ nm) for 60 min. Finally, aliquots (5 μL) of the suspensions were added to Luria-Bertani (LB) broth agar plates and cultivated at 37 °C for 24 h. As a further control, samples were treated according to the above steps, but in the dark. Subsequently, the numbers of colonies (N) were quantified. The expression for quantifying the antibacterial efficacy is as follows:

$$Relative\ bacterial\ viability\ (\%) = CFU\ sample\ /\ CFU\ control * 100\%$$

6. Intracellular ROS Detection

Oxidative stress was assessed by measuring intracellular ROS production by measuring bacterial cells with 2, 7-dichlorofluorescein diacetate (DCFH-DA). Firstly, the number of bacteria was adjusted to 1×10^8 CFU/mL, and the concentration of each sample was 2000 μg/mL. The bacterial suspensions were then mixed with aliquots (1 mL) of $Bi_4O_5Br_2$ and $Bi/Bi_4O_5Br_2$ solutions, respectively. As a control, normal saline (1 mL) was added to the bacterial suspension. All samples were vertically irradiated

using a 500 W xenon lamp (λ > 420 nm). As a further control, samples were treated according to the above steps, but in the dark. where reaction times are 25, 35, 45 and 60 minutes. Intracellular levels of reactive oxygen species were measured using reactive oxygen species assay kits (Beyotiome, China) according to the manufacturer's instructions, and the fluorescence intensity at 488 nm excitation and 525 nm emission was measured using a multifunctional microplate detector.

7. Cell Membrane Permeability Test.

Firstly, the number of bacteria was adjusted to 1×10^8 CFU/mL, and the concentration of each sample was 2000 μg/mL. The bacterial suspensions were then mixed with aliquots (1 mL) of $Bi_4O_5Br_2$ and $Bi/Bi_4O_5Br_2$ solutions, respectively. As a control, normal saline (1 mL) was added to the bacterial suspension. All samples were vertically irradiated using a 500 W xenon lamp (λ > 420 nm). The irradiation durations were set at 45 min for the *E. coli* group and 60 min for the *S. aureus* group. As a further control, samples were treated according to the above steps, but in the dark. Finally, the treated *E. coli* and *S. aureus* was blended with 7% DMSO and ONPG (3.8 μg/mL), and the OD value of the supernatant was measured at 420 nm by a microplate reader.

8. Protein Leakage Test

The bacterial suspension was prepared and processed as described in Section 7. Following treatment, bacteria were centrifuged at 8000 rpm for 5 min, and the cell-free supernatant was collected. The protein concentration in the supernatant was determined using the Bradford (Bradford Protein Assay Kit) protein quantification kit (Solarbio, China), following the steps in the instructions exactly.

9. Adenosine Triphosphate (ATP) Test

The bacterial suspension was prepared and processed as described in Section 7. Finally, the mixture was centrifuged, and the fluorescence intensity in the supernatant was detected by the enhanced ATP detection kit (Beyotime, China). Within a certain concentration range, the fluorescence production is proportional to the concentration of ATP.

10. Bacterial Photocurrent Response Testing

Initially, $Bi_4O_5Br_2$ and $Bi/Bi_4O_5Br_2$ were mixed with isopropanol at a 1:5 (v/v) ratio and ultrasonically dispersed for 15 min to obtain homogeneous suspensions. The aqueous suspensions of $Bi_4O_5Br_2$ and $Bi/Bi_4O_5Br_2$ were then dropped on SnO_2: F (FTO) substrates and dried at 60°C to form uniform films. Then, the prepared films were immersed in bacterial suspensions containing various concentrations (typically 104-10^8 CFU/mL) of *E. coli* or *S. aureus* for 1 h, followed by drying at 60°C. Finally, the photoresponse current density was measured using an electrochemical workstation (CHI760E, China).

11. Bacterial cyclic voltammetric curve experiment

Bacteria have a double-layered EPS structure in which loosely bound EPSs diffuse from the tightly bound EPSs that surround the cells. The EPS layer was electrochemically active itself and accelerated electron transfer between the cells and extracellular electron acceptors/donors. The redox reaction with EPSs was previously detected using electrochemistry technology.

Sample preparation was performed according to Section 10, with suspensions of *E. coli* and *S. aureus* adjusted to 1×10^8 CFU/mL. The electrochemical behavior was observed with a typical three-electrode system consisting of a glassy carbon electrode (4 mm in diameter), a platinum-wire counter electrode, and an Hg/HgCl reference electrode with saturated Na_2SO_4 on a CHI760E electrochemical working station

(China). The redox reaction between the $Bi/Bi_4O_5Br_2$ nanosheets and cell membranes in 0.1 M Na_2SO_4 solution was evaluated using a CV test. The parameters were as follows: Ei =−0.5 V and Ef= 0.5 V with a scan rate of 20 mV/s.

12. Supporting figures

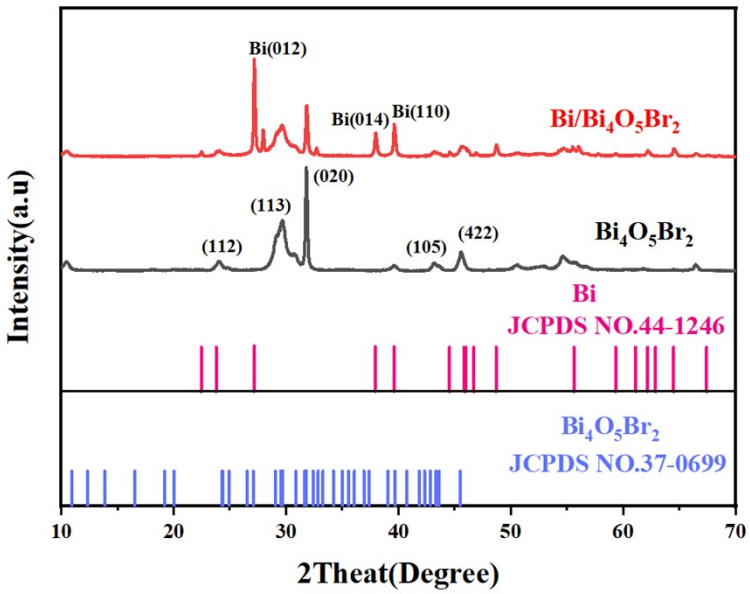

Figure S1. XRD patterns of $Bi/Bi_4O_5Br_2$, $Bi_4O_5Br_2$ and Bi.

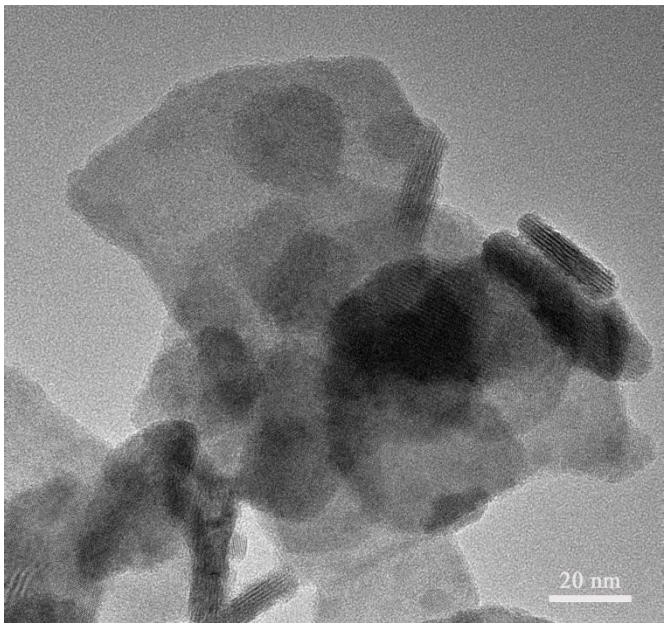

Figure S2. TEM images of $Bi_4O_5Br_2$.

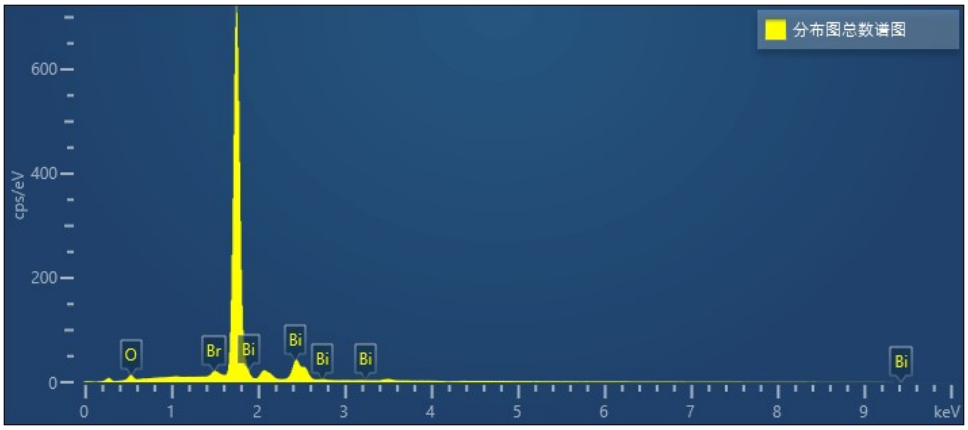

Element	O	Br	Bi
Wt%	7.61%	18.21%	74.18%
AT%	44.92%	21.53%	33.54%

Figure S3. EDS spectrum and the element composition of $Bi/Bi_4O_5Br_2$.

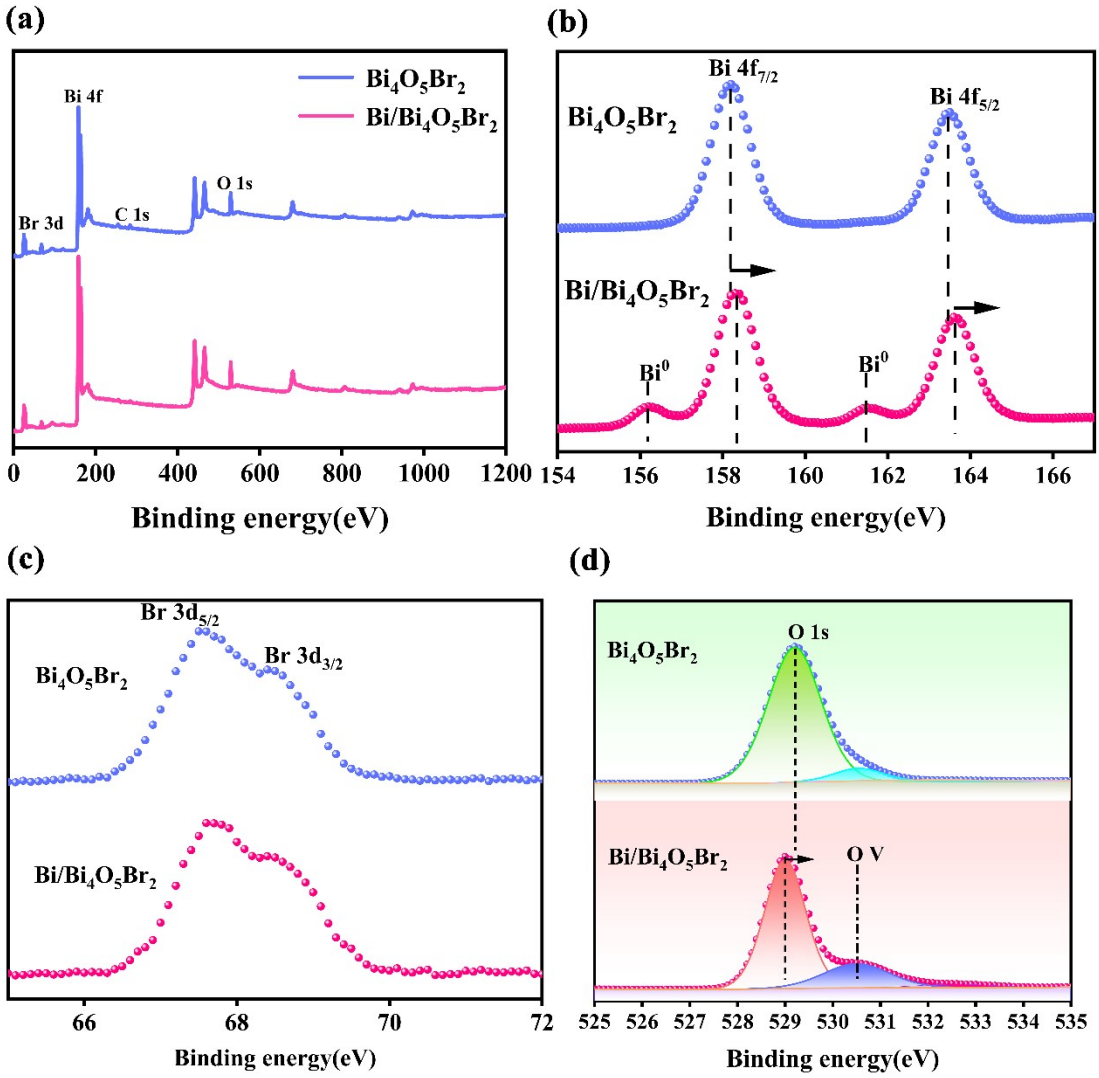

Figure S4. Characterization of the $Bi/Bi_4O_5Br_2$ ohmic-like heterojunction. (a) XPS survey spectra of $Bi_4O_5Br_2$ and $Bi/Bi_4O_5Br_2$. (b, c, d) The element spectra of the studied materials: Bi4f, Br3d and O1s.

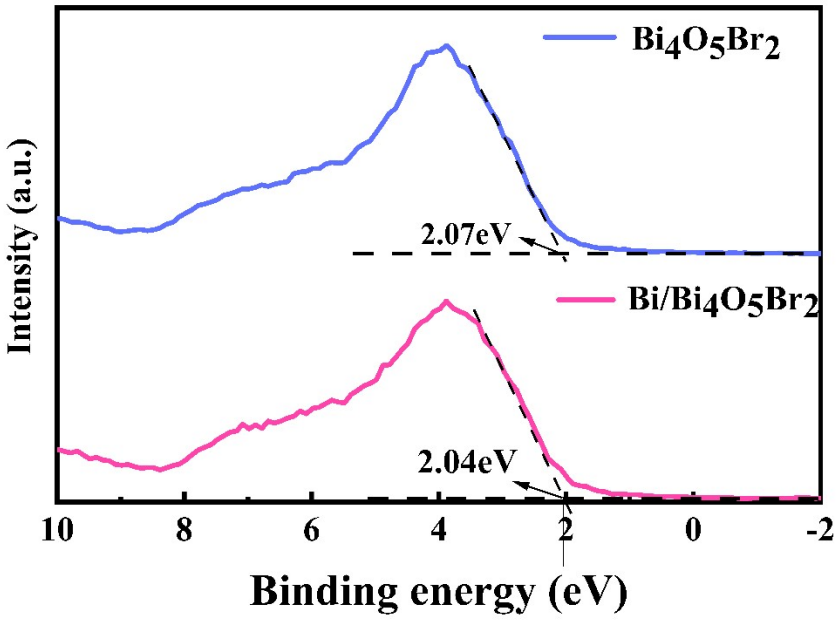

Figure S5. Characterization of the $Bi/Bi_4O_5Br_2$ ohmic-like heterojunction. UV-vis-NIR absorption spectra of $Bi_4O_5Br_2$ and $Bi/Bi_4O_5Br_2$ heterojunctions.

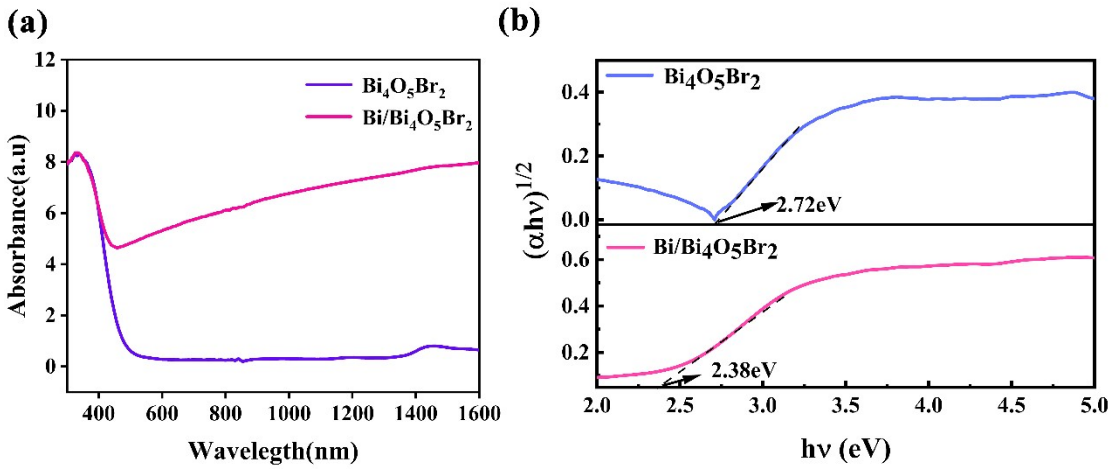

Figure S6. Characterization of the $Bi/Bi_4O_5Br_2$ ohmic heterojunction. (a) Plots of (αhν)1/2 versus hν. (b) Photocurrent testing of $Bi_4O_5Br_2$ and $Bi/Bi_4O_5Br_2$.

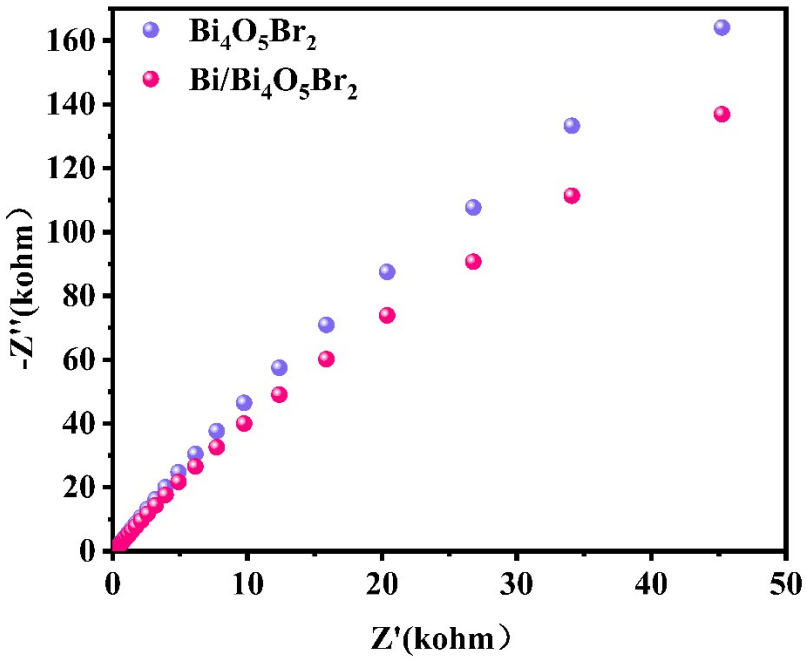

Figure S7. Electrochemical impedance spectroscopy (EIS) of $Bi_4O_5Br_2$ and $Bi/Bi_4O_5Br_2$.

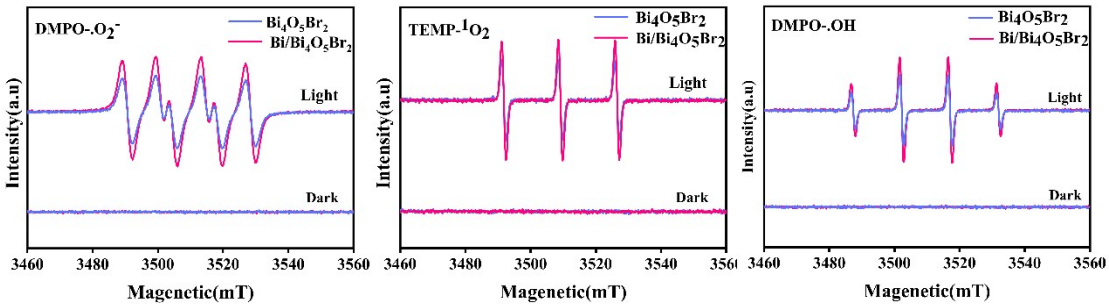

Figure S8. ESR spectra of $Bi_4O_5Br_2$ and $Bi/Bi_4O_5Br_2$ heterojunctions: DMPO-·O- 2, DMPO-·OH and TEMP-$^1O_2$.

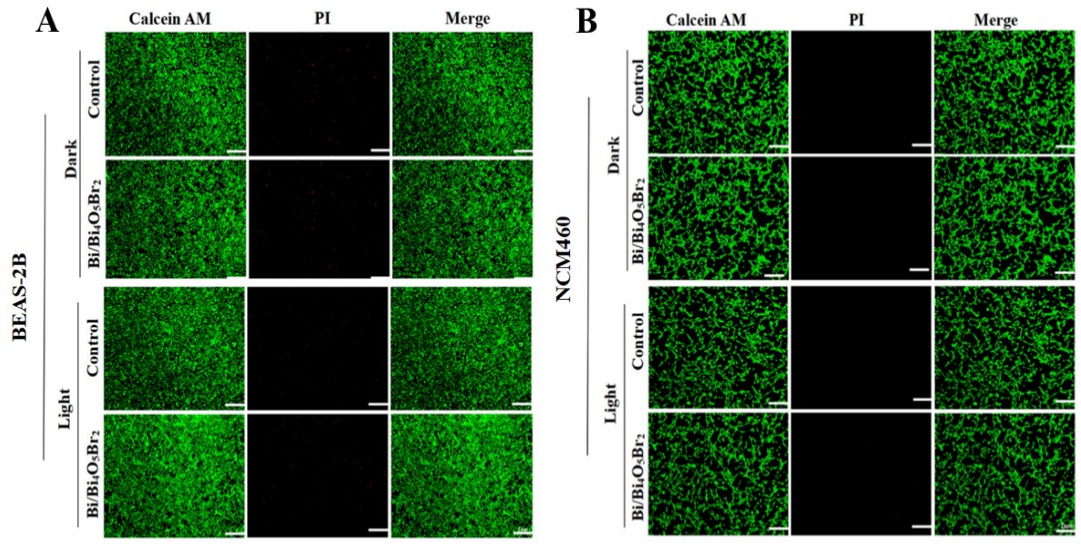

Figure S9. Biocompatibility of the $Bi/Bi_4O_5Br_2$ nanosheet heterojunctions. (a, b) Fluorescence images of BEAS-2B cells and NCM460 cells in the different groups following Live/Dead staining. Scale bar = 200 μm.

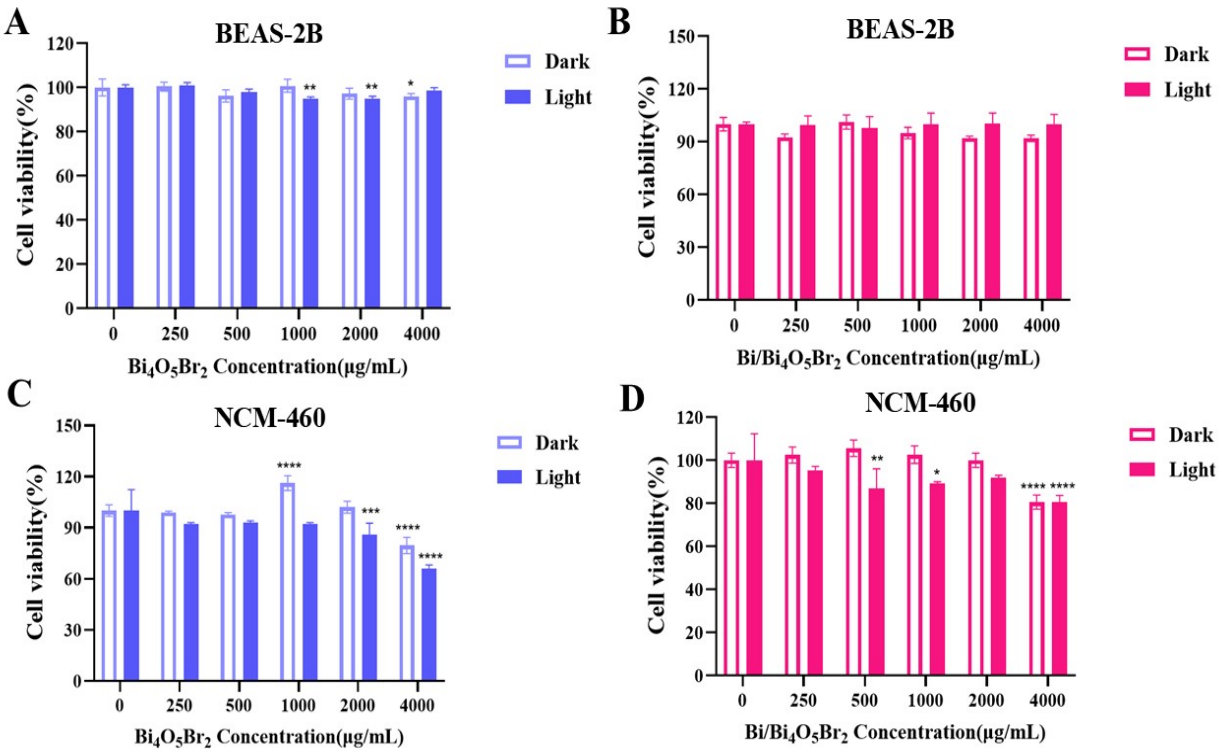

Figure S10. Cytocompatibility evaluation. (a, b) The toxicity of $Bi_4O_5Br_2$ to BEAS-2B and NCM460 measured by CCK-8 (c, d) The toxicity of $Bi/Bi_4O_5Br_2$ to BEAS-2B and NCM460

measured by CCK-8, n = 3 independent experiments per group, *$p < 0.05$, **$p < 0.01$, ****$p <$ 0.0001.

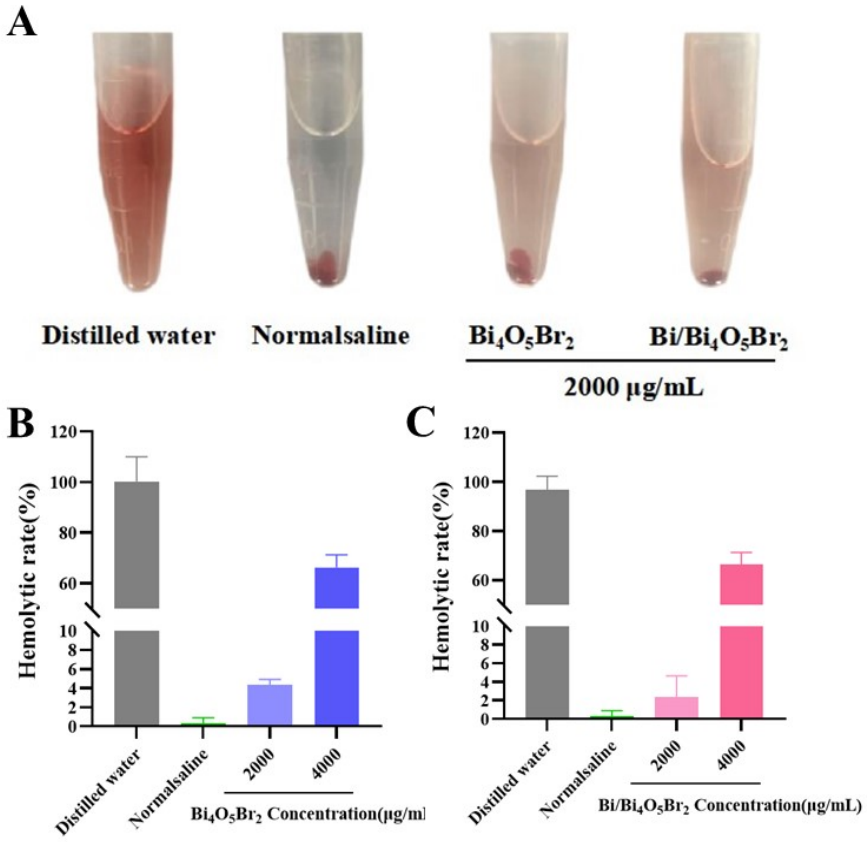

Figure S11. Cytocompatibility evaluation. (a) the hemolysis phenomenon image. (b, c) Haemolysis of erythrocytes by concentrations of 2000 and 4000 μg/mL$Bi_4O_5Br_2$ and $Bi/Bi_4O_5Br_2$.

Table S1. Comparison of the Performance of $Bi/Bi_4O_5Br_2$ and Other PDT Materials

Material System	Antibacterial Efficiency	ROS Production /Species	Light Source	Treatment Time	Biocompatibility	Ref.
This work	>95% (against *E. coli* and *S. aureus*)	Enhanced generation of •OH, $•O_2^-$, $^1O_2$	Visible light (420-800 nm)	60min	High (Low hemolysis rate, high cell viability)	
$Ag@TiO_2$ Core-Shell Nanoparticles	>95% (against *E. coli* and *S. aureus*)	High (Ag plasmonic resonance enhances local electric field, promoting ROS like •OH)	UV/Visible light	Short time (Significant effect under visible light)	——	[1]
g-C_3N_4/GO/MoS_2 Nanocomposite	>95% (against *E. coli* and *S. aureus*)	High (•OH, $•O_2^-$)	Visible light (420-550 nm)	60min	——	[2]
TiO_2/Pt	>95% (against *E. coli*)	Very high (•OH)	365 nm UV	60min	Moderate (UV toxicity)	[3]
BiOBr/ZnO	>95% (against *E. coli, S. aureus*, and *P. aeruginosa*)	Moderate (•OH, $•O_2^-$)	Visible light (420-550 nm)	120min	——	[4]
MoS_2/α-$NiMoO_4$	~100% (against *S. aureus*)	High (•OH, $•O_2^-$)	Visible light (>420 nm)	150min	——	[5, 6]

References

[1]D. Gao, F. Wang, B. Lyu et al., Multifunctional cotton fabric with durable antibacterial, superhydrophobicity, and UV resistance based on $Ag@TiO_2$ Janus nanoparticles, Res. Sq., 2023, preprint.

[2]R. Chowdhury, S. M. Aishee, N. Islam, N. Aich and S. Ahmed, Emerging two-dimensional nanomaterial and its modifications for enhanced antiviral applications: a review, R. Soc. Open Sci., 2025, **12**, 242179.
[3]V. Lazić, V. Nikšić and J. M. Nedeljković, Application of TiO_2 in Photocatalytic Bacterial Inactivation: Review, Int. J. Mol. Sci., 2025, **26**, 10593.
[4]I. Zgura, N. Badea, M. Enculescu, V. A. Maraloiu, C. Ungureanu and M. E. Barbinta-Patrascu, Burdock-Derived Composites Based on Biogenic Gold, Silver Chloride and Zinc Oxide Particles as Green Multifunctional Platforms for Biomedical Applications and Environmental Protection, Materials, 2023, **16**, 1153.
[5]R. Chowdhury, S. M. Aishee, N. Islam, N. Aich and S. Ahmed, Emerging two-dimensional nanomaterial and its modifications for enhanced antiviral applications: a review, R. Soc. Open Sci., 2025, **12**, 242179.
[6]S. K. Ray, D. Dhakal, J. Hur and S. W. Lee, Visible light driven MoS_2/α-$NiMoO_4$ ultra-thin nanoneedle composite for efficient Staphylococcus aureus inactivation, J. Hazard. Mater., 2020, **385**, 121553.